ground water

The Influence of Wellbore Inflow on Electromagnetic Borehole Flowmeter Measurements

by Tom Clemo[1], Warren Barrash[2], Edward C. Reboulet[3], Timothy C. Johnson[4], and Carsten Leven[5]

Abstract

This paper describes a combined field, laboratory, and numerical study of electromagnetic borehole flowmeter measurements acquired without the use of a packer or skirt to block bypass flow around the flowmeter. The most significant finding is that inflow through the wellbore screen changes the ratio of flow through the flowmeter to wellbore flow. Experiments reveal up to a factor of two differences in this ratio for conditions with and without inflow through the wellbore screen. Standard practice is to assume the ratio is constant. A numerical model has been developed to simulate the effect of inflow on the flowmeter. The model is formulated using momentum conservation within the borehole and around the flowmeter. The model is embedded in the MODFLOW-2000 ground water flow code.

Introduction

The use of an electromagnetic borehole flowmeter (EBF) without use of a packer (inflatable annular balloon) or skirt (stiff rubber flange) to force all the flow in a borehole through the flowmeter is recommended to overcome problems with significant and/or changing head loss across a flowmeter with packer or skirt (e.g., Ruud et al. 1999; Arnold and Molz 2000). Packers and especially skirts can have problems properly seating, which can allow significant amounts of bypass flow within the borehole; blockage of flow up the wellbore is significant—potentially making bypass flow around a borehole screen significant (Dinwiddie et al. 1999); and packer inflation/deflation and skirt positioning are more time consuming than operating a flowmeter with only a centralizer. In our study of the Boise Hydrogeophysical Research Site (BHRS) (Barrash and Knoll 1998), we want to provide a detailed characterization of the inflow to many boreholes at a fine vertical scale to estimate the vertical distribution of hydraulic conductivity in the aquifer.

We experimented with three configurations of the flowmeter for the borehole measurements. Initially, we used the flowmeter with a skirt of overlapping flaps to divert all flow through the flowmeter, but measurements were noisy and not very repeatable at pumping rates appropriate for avoiding bypass flow (Dinwiddie et al. 1999) because the skirt did not form a complete seal and the flowmeter was not always vertically oriented. We also tried using the flowmeter with an inflatable packer to divert all the flow through the flowmeter, but also with this configuration the measurements were noisy compared with the incremental flow rate differences occurring at overall pumping rates appropriate for avoiding significant bypass flow. To get repeatable and generally monotonically increasing (i.e., not noisy) incremental flow rate measurements with successive upward measurement positions (while avoiding bypass flow outside the well), we used the flowmeter with a centralizer instead of a skirt or packer (Ruud et al. 1999; Arnold and Molz 2000).

[1]Corresponding author: Center for the Investigation of the Shallow Subsurface, Boise State University, 1910 University Dr., Boise, ID 83725-1536; Now at: 141 Tipsue Rd.,Livingston, MT 59047; (406) 223-5882; tomc@cgiss.boisestate.edu

[2]Center for the Investigation of the Shallow Subsurface, Boise State University, 1910 University Dr., Boise, ID 83725-1536

[3]Kansas Geological Survey, 1930 Constant Ave., Lawrence, KS 66047-3726

[4]Idaho National Laboratory, P.O. Box 1625, Idaho Falls, ID 83415-2107

[5]The Helmholtz Centre for Environmental Research—UFZ, Permoserstraße 15, 04318 Leipzig, Germany

Received May 2008, accepted January 2009.

doi: 10.1111/j.1745-6584.2008.00559.x

For this configuration, we used a relatively high pumping rate (1.6×10^{-3} to 1.9×10^{-3} m^3/s) to provide incremental flow rate increases, which, though small (because much of the flow bypassed the flowmeter in the annular space outside the flowmeter and inside the well), were greater than the noise. Discussions with other flowmeter users over the years indicated that this operational configuration has been adopted by some for similar reasons, and this configuration is one of the recommended configurations by the manufacturer (Century Geophysical Corp. 2002). Data acquired using a packer and acquired in the absence of a packer are compared in Figure 1. The data from a centralized EBF indicate a mostly monotonic increase in flow, as would be expected from continual inflow to the well. The data from a packed-off EBF indicate a large noise level that causes the data to be nonmonotonic.

The measurements without a skirt, however, showed an increase in measured flow within blank casing at joints between screen sections in the wells at the BHRS, where inflow cannot occur, and an apparent decrease in inflow to the well just below the casing breaks. The primary goal of the work described in this paper was to determine why. We have found that the calibration of a flowmeter used without a skirt or packer is sensitive to flow entering the borehole above the entrance of the flowmeter. A secondary goal of the work was the development of a numerical model that could be used to simulate the flowmeter behavior. This model provides a basis for inferring aquifer hydraulic conductivity from the flowmeter measurements.

In presenting our findings at conferences, we have found that use of the flowmeter with a centralizer only, rather than with a packer or skirt, is common, and the anomalous behavior (see Figure 2) is recognized by others. In this paper, we present both laboratory and modeling investigations of the use of a flowmeter without a skirt or packer. Throughout the rest of this paper when we refer to the flowmeter, it is used to connote an EBF with a centralizer instead of a packer or skirt.

The field evidence prompting this study comes from EBF measurements in wells at the BHRS. The BHRS is

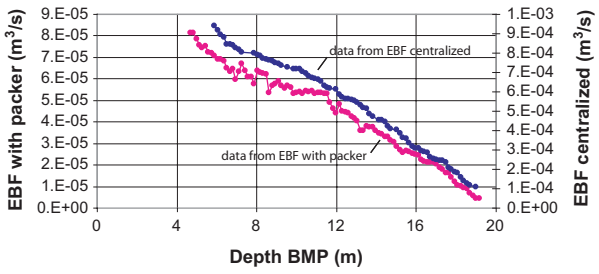

Figure 1. Comparison of EBF measurements for the same well using a packer (lower data set; left axis) and with a centralizer (upper data set; right axis). The measurements with a packer are more noisy, probably due to much smaller flow rates. Note that the pumping rate was over an order of magnitude larger when the centralizer data were acquired (right axis). Data shown here are full-recorded flow rates, not net flowrates following removal of ambient flow.

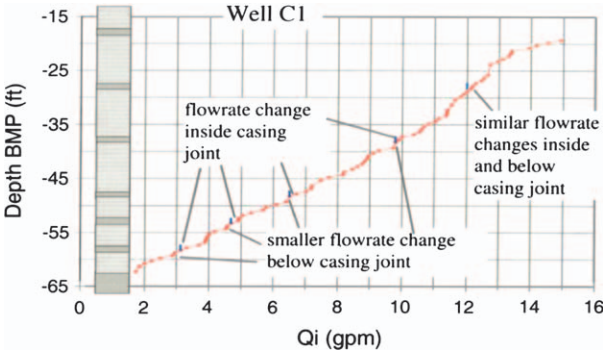

Figure 2. Example of anomalous flowmeter measurements.

located in a gravel bar alongside the Boise River approximately 15 km east of downtown Boise, Idaho. The shallow unconfined aquifer there consists of coarse-grained fluvial deposits underlain by clay (Barrash and Reboulet 2004). The site was established to aid development of geophysical techniques for characterizing subsurface properties (Barrash et al. 1999; Clement et al. 1998). A core, drive, and drill technique was used to construct the wells at the BHRS with minimal disturbance of the formation including natural collapse of the formation against the well screen after removal of the drive casing (e.g., Morin et al. 1988). Collapse of the formation against the polyvinyl chloride (PVC) screen was anticipated, then confirmed with vertical seismic profiling (Michaels 1998, 2001). The potential for small regions of incomplete collapse makes bypass flow around blockage of the borehole by a packer or skirt an issue. The aquifer is screened throughout its 15 to 17 m thickness. Additional details of well construction and cleaning are given in Barrash et al. (2006).

Figure 2 presents flowmeter measurements from 1 of the 13 wells of the central well field at the site. The figure plots measured flow vs. depth. Depth is measured from a marker at the top of the casing. To the left of the plot is a schematic diagram of the screen for this well. Casing joints where two sections of screen are connected are depicted by solid bands. At the bottom of the diagram, the clay layer is also depicted as a solid section of the screen. These are regions where there is no inflow. The plot is annotated to point out two aspects of anomalous behavior: (1) measured flow increases occur in the casing joints and (2) markedly reduced flow increases occur just below the joints. In a few instances, a decrease in measured flow occurs below the joints. These are not shown in the figure.

To develop an understanding of the influence of casing joints on the flowmeter measurements, we first created a physical simulator of a BHRS-like well in the laboratory. Having recreated flowmeter behavior similar to the field response to casing joints, we then proceeded to develop a numerical model of fluid flow through and around a flowmeter in a well and coupled this to an aquifer flow model. In the following sections, we describe the laboratory calibration of the flowmeter, first in a solid wall pipe and then in the well screen of the aquifer simulator. Next, we provide a brief background on simulating vertical fluid flow

in an open borehole and special aspects of simulating flow in and around the flowmeter. A description of the coupled flowmeter-aquifer model of the laboratory simulator is then presented followed by the results of simulating one laboratory experiment. With flow theory and modeling results established, we describe the physical phenomena that are causing the behavior we see in the field.

Calibration Experiments

Solid Pipe Model Calibration

Initial calibration check of the EBF tool was run in a solid wall 10 cm inner diameter (ID) PVC pipe. Our calibration setup and measurement procedures were similar to those of the manufacturer (Century Geophysical Corp., Tulsa, Oklahoma, http://www.century-geo.com). The calibration was conducted over 2 orders of magnitude in flow rate. Figure 3 presents the ratio of measured flow in the flowmeter to total flow in the pipe plotted as a function of pipe flow rate on a log scale. Data from the flowmeter are plotted using symbols. The calibrated model that we present later is drawn with a solid line. There are two distinct regions in this plot, which characterize the response of the flowmeter: (1) when the flow is laminar at low flows and (2) when the flow is turbulent at higher flows. The range of pipe flows between 2.3×10^{-4} and 2.7×10^{-4} m^3/s is a transition region where flow may oscillate between laminar and turbulent conditions (Siwoń 1987; Eckhardt et al. 2007; Rouse 1961). The fact that the ratio is nearly constant more than 90% of the flow range is masked by the logarithmic ordinate; instead, the figure accentuates changes from a constant ratio of measured flow through the flowmeter to total flow in the pipe.

At zero flow in the pipe, the flowmeter produces a signal that indicates a negative flow rate. At small flow rates, if this negative flow at zero is subtracted from the reported flow, as the manufacturer recommends, it very effectively linearizes the response in the low flow region. That is not our purpose. We have added a 1.6×10^{-6} m^3/s offset to the data, which is less than the average zero flow signal, but makes the readings near 1.0×10^{-5} m^3/s positive. Selecting and including this offset were part of the model calibration.

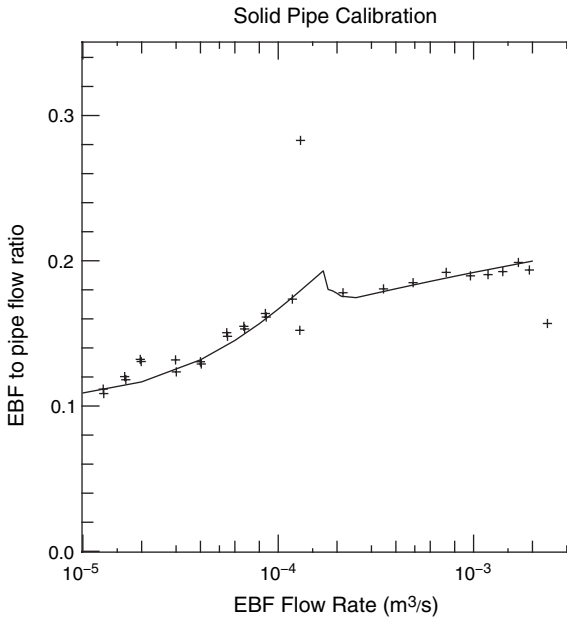

Figure 3. Flowmeter measurements from solid pipe calibration (symbols) and calculated flowmeter response (line).

Screened Pipe Model Calibration

We constructed a borehole-aquifer simulator in a laboratory building. The simulator consists of three concentric PVC pipes (Figure 4a). The inner pipe is composed of two 3.05-m sections of 10 cm ID, 11.43 cm outer

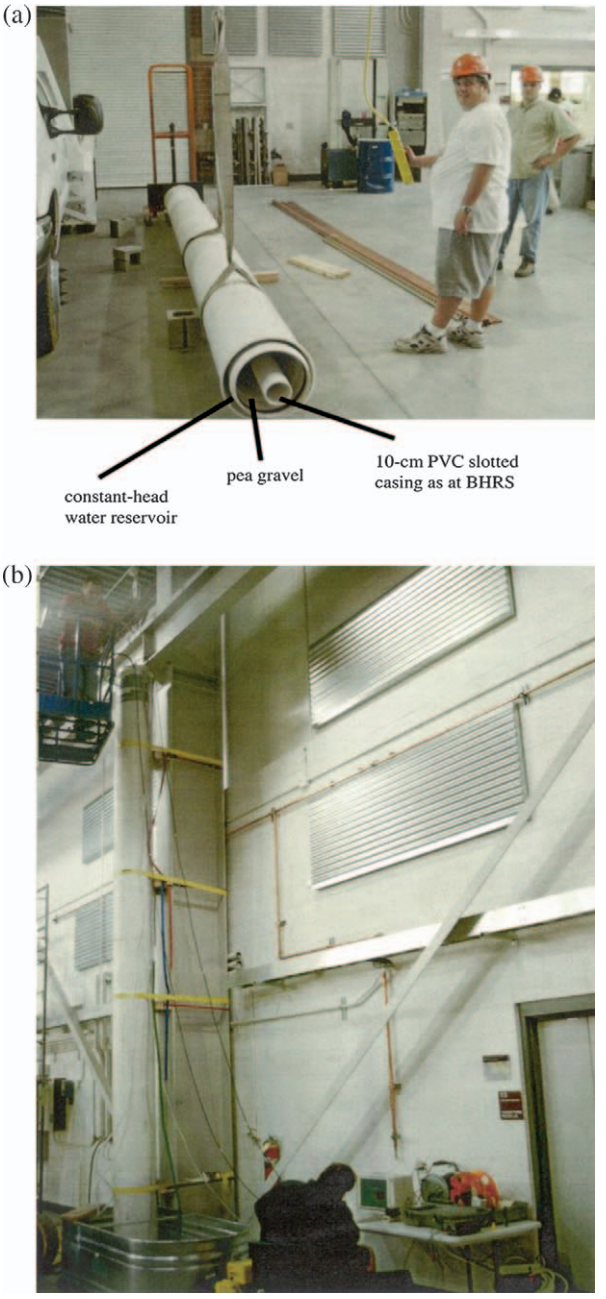

Figure 4. (a) Borehole-aquifer simulator and (b) simulator configuration during experiments.

diameter (OD) Schedule 40 PVC screen. A solid casing joint (~0.3 m long) occurs where the two sections are connected. The central pipe is a 25.4 cm ID, 26.8 cm ODm solid PVC pipe that was perforated with horizontal sawn slots. The annular space between the screen and the central pipe was filled with pea gravel (~4 mm diameter). The outer pipe is a 30.5 cm ID solid PVC pipe that serves as a reservoir supplying fluid to the central region at relatively uniform head. Each pipe was sealed at the bottom. The three pipes were then placed vertically in a high-bay building (Figure 4b). The casing joint between the inner pipe screen sections occurs over the elevation interval from approximately 2.9 to 3.2 m from the bottom of the simulator.

Water was pumped at a nominally constant rate from the upper portion of the screen and supplied to the reservoir at a rate that maintained a slight overflow at the top on the simulator. Flowmeter measurements were taken at either 0.15- or 0.31-m intervals depending on experiment and in some cases, at the top and bottom of the casing joint also. The pumping rate was monitored by volumetric methods, that is, measuring the time to fill a calibrated cylinder (lower flow rates) or a bucket (higher flow rates).

Fifteen experiments were performed over a range of pumping rates from 5.3×10^{-4} to 8.7×10^{-4} m^3/s. When increased proportionally to account for the aquifer thickness and longer screened interval, the range of flow rates spans those used at the BHRS. The results of these experiments are not fully consistent in that some runs have different flowmeter measurements at nearly identical flow rates. We are convinced that the inconsistencies are not due to large errors in measurement (because flow rate measurements were repeated at each elevation per run) or in data processing (because data management and treatment have been checked). Future efforts will consider ways to improve the essentially reconnaissance experimental design used here; several suggestions are included in the Discussion section.

Figure 5a depicts a representative sample of the experimental data. This sample does not show the most consistent results nor the most extreme cases of inconstancy. Our point in presenting these data is to demonstrate the very close fit obtained by the numerical model shown in Figure 5b is better than the reliability of the data themselves. The figure presents flow rate measured by the flowmeter for different elevations of the entrance of the flowmeter. A vertical shaded region is drawn where the casing joint occurs. Despite the inconsistencies, all the experiments show the anomalous behavior similar to what is seen in the field data. In these experiments, the measured flow increases across the casing joints and the measured flow decreases below the casing joint. The decrease in measured flow occurs when the top of the flowmeter barrel enters the casing joint.

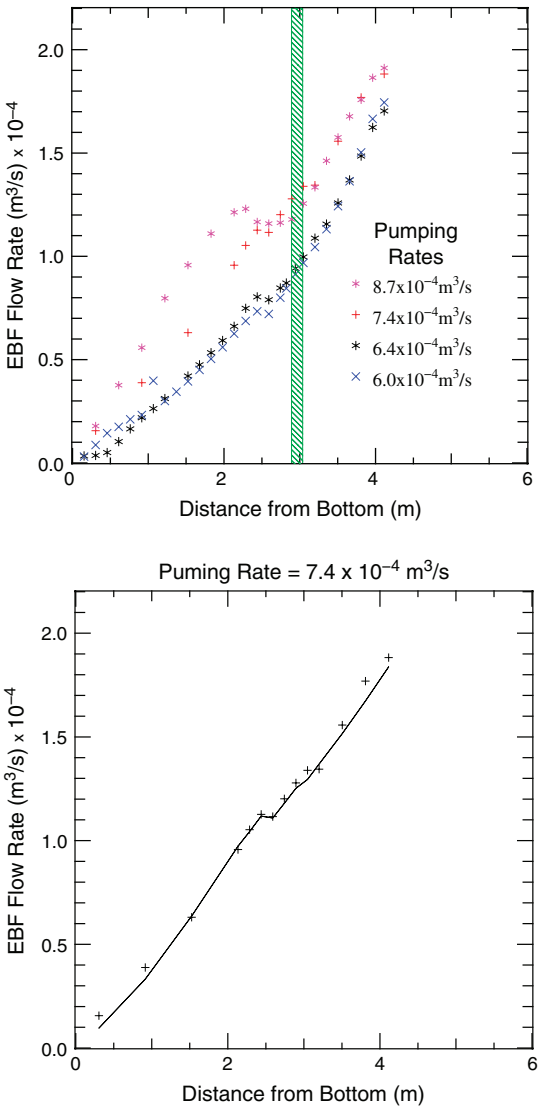

Figure 5. (a) Selected experimental data sets. The shaded vertical line indicates the position of the casing joint and (b) data (symbols) and calculated flowmeter response (line).

Flow Theory

In this section, we present the theoretical basis for numerically modeling flow in and around the flowmeter. Figure 6 shows some of the different flow conditions simulated. Location A in the figure has flow in an open borehole. At location B, flow is within the screened wellbore and around the flowmeter barrel. Location C has flow inside the flowmeter barrel and is simulated using traditional pipe flow equations. At location D, flow exits the flowmeter barrel past bars joining a connecting rod to the flowmeter barrel and flow here rejoins the flow around the outside of the barrel. Above this is annular flow around the connecting rod.

The development of in-well flow hydraulics is based on momentum conservation. Momentum conservation is a restatement of the relation $F = ma$. The change in momentum across a borehole section is depicted in Figure 7. In Figure 7, z_1 and z_2 are elevations and P_1 and P_2 represent the fluid pressure at the bottom and top of the control volume, respectively; r_w is the radius of the wellbore; $P(z)$ is the vertical pressure distribution; v_z represents a radially dependent vertical velocity distribution within the borehole; v_b is the bulk velocity of the flow in

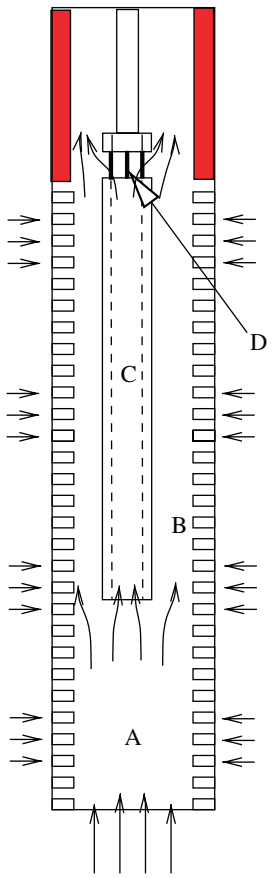

Figure 6. Regions of different flow conditions: location A, flow in an open borehole; location B, flow around the flowmeter barrel; location C, flow inside the flowmeter barrel; location D, flow exiting the flowmeter barrel.

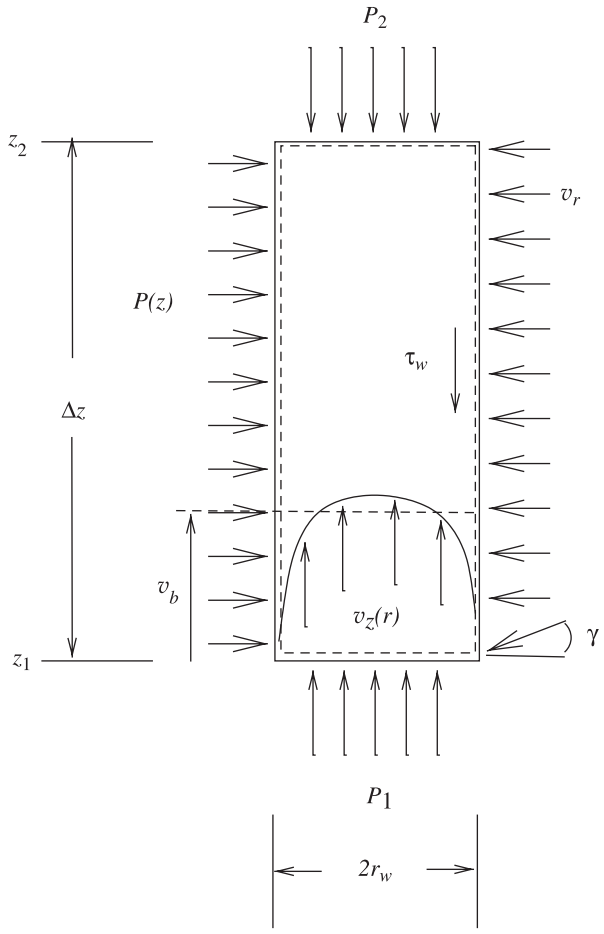

Figure 7. Momentum balance control volume for a wellbore.

the wellbore, which is defined as the average over the cross-sectional area of the borehole; and v_r is the radial velocity just inside the screen. While written with a radial direction subscript, the radial velocity may vary from horizontal by an angle γ. τ_w represents shear forces operating on the fluid at the wall of the screen. The average or bulk velocity is defined as:

$$v_b = \frac{1}{\pi r_w^2} 2\pi \int_o^{r_w} v_z r \, \mathrm{d}r \tag{1}$$

The momentum equation for a volume of fluid is (Parker et al. 1969):

$$\frac{D}{Dt} \int_{\mathrm{Vol}} \rho v \, \mathrm{d}(Vol) = \sum F_i \tag{2}$$

where ρ is the density of fluid, v is the velocity, F_i are external forces, and D/Dt is the substantial derivative. The substantial derivative is the total derivative with respect to a moving body of fluid, for example, in the Lagrange reference frame, and is defined by $\frac{Dp}{Dt} = \frac{\partial p}{\partial t} + v_r \frac{\partial p}{\partial r} + v_z \frac{\partial p}{\partial z}$. Equation 3 separates the substantial derivative into two components: the change in internal momentum within the volume and the flux of momentum across the boundaries of the volume.

$$\frac{D}{Dt} \int_{\mathrm{Vol}} \rho v \, \mathrm{d}(\mathrm{Vol}) = \frac{\partial}{\partial t} \int_{\mathrm{Vol}} \rho v \, \mathrm{d}(\mathrm{Vol}) + \int_{\Omega} \rho v (v \cdot n) \mathrm{d}\Omega \tag{3}$$

The conservation of momentum is a vector equation, which must be satisfied in each direction. Axial symmetry assures agreement in the radial direction. With the assumption of steady incompressible flow, the first term on the right-hand side of Equation 3 is zero and the derivative can be rewritten for the axial direction as follows:

$$\frac{D}{Dt} \int_{\mathrm{Vol}} \rho v \, \mathrm{d}(\mathrm{Vol}) = \rho 2\pi \int_o^{r_w} v_z^2 r \, \mathrm{d}r \Big|_{z_2} - \rho 2\pi \int_o^{r_w} v_z^2 r \, \mathrm{d}r \Big|_{z_1} + \rho 2\pi r_w \int_{z_1}^{z_2} v_z \cdot v_r \mathrm{d}z \tag{4}$$

The first two terms on the right-hand side of this equation are momentum flux across the top and bottom boundaries, respectively. The last term accounts for momentum flux in the axial direction from flow entering the borehole along the sides.

The forces acting on the fluid in Equation 2 are gravity, pressure around the boundaries, and shear along the sides.

$$\sum F = -\rho g \pi r_w^2 \Delta z + \pi r_w^2 (P_1 - P_2) - \pi 2 r_w \int_{z_1}^{z_2} \tau_w \mathrm{d}z \tag{5}$$

As developed in the Appendix and in much greater detail in Clemo (2009), the head drop across a section with inflow through the sides can be written as:

$$\Delta h = \int_{z_1}^{z_2} f \frac{v_b^2}{4 r_w g} \mathrm{d}z + \beta_2 \frac{v_{2b}^2}{g} - \beta_1 \frac{v_{1b}^2}{g} + \frac{2}{r_w g} \int_{z_1}^{z_2} v_z \cdot v_r \mathrm{d}z \tag{6}$$

where f is the friction factor and β relates momentum flux to the average fluid velocity, v_b. From the investigation of Siwoń (1987) of the influence of inflow on head drop, Equation 6 can be written as:

$$\Delta h = f_s \frac{v_b^2}{4 r_w g} \Delta z + \beta_2 \frac{v_{2b}^2}{g} - \beta_1 \frac{v_{1b}^2}{g} + \frac{(\eta - 1)}{g} (v_{b2}^2 - v_{b1}^2) \tag{7}$$

where f_s includes the influence of screen slots on fluid shear along the sides and η, which is a function of inflow rate at low inflow, encapsulates the influence of inflow on both the wall shear and the axial momentum flux of radial flow (Clemo 2006). The specific influence of inflow on shear or inflow momentum flux could not be separated in Siwoń's experiments.

Flowmeter Modeling

Placement of the flowmeter in a well creates vertical annular flow around the flowmeter in addition to pipe flow in the well and through the flowmeter barrel. The variation in geometry of the flowmeter also causes abrupt changes in the cross-sectional area of the borehole that is open to flow. The flowmeter we have been using was manufactured by Century Geophysical Corp. Figure 8 is a schematic diagram of the flowmeter. It is 1.5 m long with a measurement barrel that is 0.42 m long. The lower section of the barrel is 2.54 cm ID and 5.1 cm OD with a rounded entryway. The barrel ID expands to 4.32 cm with a 1.54 cm diameter post protruding into it from the connecting rod. The connecting rod is attached to the barrel by three welded struts.

Modifications to the open borehole conceptual and numerical models include annular flow past the outside of the flowmeter barrel and connecting rod, the effects of diameter changes of the connecting rod, separation of flow into and around the barrel, momentum losses associated with flow out of the barrel and merging of this flow with the bypass flow around the flowmeter, and flow within the barrel including the effect of the barrel expansion and protruding rod (Figure 8). We do not have a complete theoretical description of the influences of all these factors. Subsequently, we describe our understanding of the head drops associated with these features. The model is constrained by this understanding, but the final model is empirically based on fitting of the model predictions to our experimental data. A comparison of the fitted model to the experimental data is shown in Figure 5b.

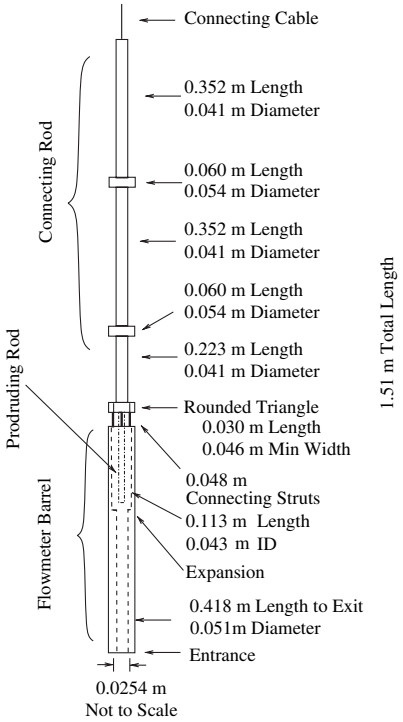

Figure 8. Schematic diagram of EBF.

Minor Losses from Expansion and Contraction

The fluid velocity must either accelerate for contractions or decelerate for enlargements when the cross-sectional area of the open part of the borehole changes due to changes in flowmeter geometry (Figure 8). These processes result in additional losses that are well established in the fluid mechanics literature for simple geometries. These losses can typically be represented as:

$$\Delta h = C \frac{v_b^2}{2g} \tag{8}$$

where velocity is determined for the smaller area, A_1. For sudden enlargements (Crane Co. 1988):

$$C = \left(1 - \frac{A_1}{A_2}\right)^2 \tag{9}$$

and for sudden contractions:

$$C = 0.5\left(1 - \frac{A_1}{A_2}\right) \tag{10}$$

These equations are used for changes in flowmeter geometry except at the entrance and exit. The entrance to the tool is rounded causing a smaller contraction loss.

Contraction losses for gradual contractions are defined (Crane Co. 1988) as:

$$C = 0.8\sin(\tfrac{\Theta}{2})(1-\tfrac{A_1}{A_2}) \text{for } \Theta \le 45^\circ$$
$$= 0.5\sqrt{\sin(\tfrac{\Theta}{2})}(1-\tfrac{A_1}{A_2}) \text{for } 45^\circ < \Theta \le 180^\circ \quad (11)$$

Unfortunately, the angle of contraction Θ is poorly defined for the rounded entrance. An arbitrary value for C of 0.4 is used in the calibration. This corresponds to an effective angle of 43°, which seems reasonable to us. The calibration of the model was not very sensitive to the coefficient for entrance losses. Consequently, the value for C was not used as a fitting parameter.

The exit of the barrel of the flowmeter is another place where special consideration is needed. The flow impinges on the base of the connecting rod and then passes in between the connecting struts. A wire screen with large openings has a loss coefficient near 1.0 (Crane Co. 1988). Passage in between the struts combined with the redirection of flow suggests a loss coefficient of at least 1.0. The model calibration established a value of 1.5.

Flow through Flowmeter Barrel

There is no radial inflow inside the flowmeter barrel. A composite equation for the entire barrel is:

$$-\Delta h = f\frac{v_{\text{fm}}^2\Delta z}{4r_{\text{fm}}g} - \beta_1\frac{r_{\text{fm1}}^2}{r_{\text{fm2}}^2}\frac{v_{\text{fm1}}^2}{g} + \beta_2\frac{v_{\text{fm2}}^2}{g} + l_{\text{ent}}\frac{v_{\text{fm1}}^2}{2g} + l_{\text{exp}}\frac{v_{\text{fm1}}^2}{2g} + l_{\text{ext}}\frac{v_{\text{fm2}}^2}{2g} \quad (12)$$

where the first term on the right-hand side represents the effect of wall shear. It has been simplified in the equation to avoid complications introduced by the changing geometry and stud protruding from the connecting rod (Figure 8). The shear term is considered to be known with the friction factor described by the widely used Colebrook-White formula (Rouse 1961). The fm subscript denotes flow in the flowmeter and 1 and flowmeter 2 refer to the entrance and following expanded regions, respectively (Figure 8). The second term represents the momentum flux through the barrel entrance. The momentum factor is multiplied by the ratio of cross-sectional areas of the two sections. The third term is momentum flux at the exit of the flowmeter barrel. This is calculated just prior to exiting the barrel. The entrance momentum factor, β_1, is unknown. l_{ent}, l_{exp}, and l_{ext} are loss coefficients for the entrance, expansion within the flowmeter, and exit, respectively.

It was not possible to fit any of the experimental data with head loss formulated using Equation 12. We were able to provide an excellent fit to one of the data sets using a transformation of the entry momentum flux based on the bulk velocity of the incoming stream from the borehole rather than based on the bulk velocity of the barrel entry—indicating that β_1 is not constant. A rationale for a variable β_1 is that the velocity profile is not fully developed at the entry to the flowmeter and as a consequence, momentum flux is not a constant function of velocity squared. The second term in Equation 12 was changed to:

$$\beta_c\frac{r_c^2}{r_{\text{fm2}}^2}\frac{v_b^2}{g}$$

Here, v_b is the bulk velocity of the wellbore at the entrance to the flowmeter and r_c represents the capture radius in the borehole below the flowmeter. Our investigation reveals that about 20% of the flow enters the flowmeter in the solid pipe calibration and up to 40% of the flow in the borehole goes through the flowmeter in the experiments with inflow through the well screen. r_c is approximately $\sqrt{2}$ larger with inflow. The combined constant factor $\beta_c r_c^2/r_{\text{fm2}}^2$ was used as the fitting parameter for this variable flow entry effect in the calibration. We were not successful in calculating a constant term for β_c when r_c^2 was calculated from the flow through the flowmeter barrel. The fitted coefficient values of the modified Equation 12 are presented in Table 1. The fit to flow in the solid pipe has been presented in Figure 3. The fit to one experiment with the screened pipe is shown in Figure 5b. Figure 5b presents measured flow in the flowmeter as a function of distance from the bottom of the laboratory simulator. From this fit, we determine that the ratio of flow in the flowmeter to flow in the screened pipe varied from 28% to 40%. The turbulent factor $\beta_c r_c^2/r_{\text{fm2}}^2$ is the most important fitted parameter controlling the magnitude and overall shape of the predicted flow. Only the lowest two measurements are in the laminar flow regime, and no measurements occur in the transition

Table 1
Fitted Coefficients

	$\beta_c r_c^2/r_{\text{fm2}}^2$	$\beta_2 + l_{\text{ext}}$	l_{ent}	β_{bp1}	$\beta_{\text{bp2}} + l_{\text{bp ext}}$	η
Solid—laminar	3.2	1.2	0.4[1]	1.18[1]	1.2[1]	—
Solid—turbulent	2.6	1.05	0.4	1.0[1]	1.05[1]	—
Screened—laminar	7.4	1.2	0.4[1]	0.59	1.2[1]	1.86[1]
Screened—turbulent	9.4	1.05	0.4[1]	0.5	1.2	14.9

[1]Coefficient was not adjusted in calibration.

region. The dip in measured flow starting at 2.5 m from the bottom is controlled by the Siwoń η factor as discussed in the next section.

Annular Flow

The equation describing head loss along the annular flow region between the flowmeter and the screen can be written:

$$-\Delta h = 1.05\left(f_s\frac{v_{\mathrm{bp}}^2\Delta z}{4r_w g} + f\frac{v_{\mathrm{bp}}^2\Delta z}{4r_{\mathrm{fmOD}}g}\right) - \beta_{\mathrm{bp1}}\frac{v_b^2}{g}\frac{r_w^2 - r_c^2}{r_w^2 - r_{\mathrm{fmOD}}^2} + \beta_{\mathrm{bp2}}\frac{v_{\mathrm{bp2}}^2}{g} + (\eta - 1)\frac{v_{\mathrm{bp2}}^2 - v_{\mathrm{bp1}}^2}{2g} + l_{\mathrm{bp\ ent}}\frac{v_{\mathrm{bp1}}^2}{2g} + l_{\mathrm{bp\ ext}}\frac{v_{\mathrm{bp2}}^2}{2g} \quad (13)$$

The first term on the right-hand side of Equation 13 is the shear term for the screen without adjustment for inflow and shear along the outside of the flowmeter. The factor of 1.05 is an adjustment for annular flow (Engineering Sciences Data Unit 1979). The subscript bp indicates flow in the annular bypass space between the outside of the flowmeter and the well screen. The outer radius of the flowmeter barrel is indicated by r_{fmOD} and Δz is the length of the barrel. The second term is the entry momentum flux of flow bypassing the flowmeter in the annular space. Like the entry momentum flux to the flowmeter barrel, it is written as a function of the bulk velocity of the borehole flow below the entrance to the flowmeter. The third term is the momentum flux at the exit of the bypass region. The fourth term represents both the influence of inflow on the shear term and the axial momentum flux of the inflow. The last two terms are entrance and exit losses for the annular bypass region.

As with Equation 12, coefficients in Equation 13 are found by fitting the experimental data acquired from the borehole-aquifer simulator. The data are not sufficient to uniquely determine all the coefficients. The shear friction factors (first term) are assumed to be well known. The exit loss term and exit momentum flux both depend on the square of bulk exit velocity. We have determined a single coefficient for these two terms. Similarly, the entrance loss and inlet momentum flux have similar but not identical dependence of bulk velocity. The term for inlet momentum flux has been used to represent both terms. Three coefficients are fitted: β_{bp1}, $\beta_{\mathrm{bp2}} + l_{\mathrm{bp\ ext}}$, and η.

Separate coefficients were found for both laminar and turbulent flow (Table 1). The transition from laminar to turbulent flow occurred near 1 m from the bottom of the simulator, so the laminar coefficients are neither well defined nor very important to this investigation. The momentum factors, β, seem to be reasonable values considering that they also represent the loss terms. The η term is eight times larger than Siwoń (1987) determined for an open pipe. The value of η has the largest influence on the magnitude of the modeled shift in measured flow apparent in Figure 5b. Therefore, it is well constrained.

Physically, in an open borehole, inflow pushes the flow toward the center of the wellbore, causing β to increase as a function of the inflow rate (Olson and Eckert 1966; Clemo 2006). In Olson and Eckert's experiments, the momentum factor reached a value of 1.11 at high inflow compared with 1.02 without inflow. The transition from the velocity profile without inflow to the profile with inflow is rapid, so establishing the profile over the length of the flowmeter is not an issue. We are not aware of any studies of the effect on β of inflow entering an annular flow stream. If we assume that the exit losses are small, the expected value of $\beta_{\mathrm{bp2}} + l_{\mathrm{bp\ exp}}$ for laminar flow without inflow would be 1.2, and the value of $\beta_{\mathrm{bp2}} + l_{\mathrm{bp\ exp}}$ for turbulent flow without inflow should be slightly larger than the value for an open borehole, approximately 1.05. The fitted value for both laminar flow and turbulence is 1.2. This indicates significantly stronger peaking in the turbulent velocity profile as one would expect for an annulus compared with an open pipe. Therefore, a significantly larger η factor, which incorporates the momentum factor increase in a net effect, is also expected.

Implementation

The borehole flow model presented here has been incorporated into the axially symmetric version of MODFLOW-2000 (Harbaugh et al. 2000) documented by Clemo (2002). The method of merging the momentum conservation equations into MODFLOW-2000 is presented in Clemo (2009). The three inner columns of the axially symmetric MODFLOW model are used to simulate flow in and around the flowmeter (see Figure 9). The three columns may represent an open borehole, the flowmeter barrel, or the connecting rod above the barrel. The latter two are shown as shaded regions in Figure 9. Column 4 represents the well screen and the outer columns represent the aquifer. The axially symmetric model is two dimensional; columns define radial positions and layers define depth. Changes in the geometry of the flowmeter

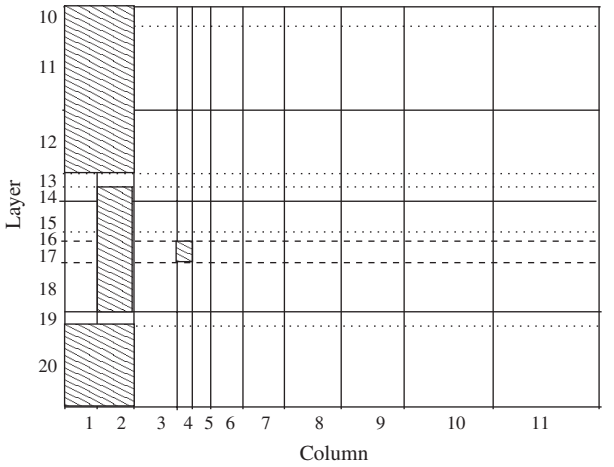

Figure 9. Example discretization of model. Shaded regions above layer 19 represent no flow regions of the flowmeter or in the case of column 4 a blank section of well screen and below layer 19, columns 1 and 2 are not part of the model and the inner diameter of column 3 set to 0.

are accommodated by specifying the radial position of each cell boundary separately. Where the flowmeter is absent, the two innermost columns are made inactive and the third column is given a zero inner radius and an outer radius at the edge of the screen. For model layers where the connecting rod above the flowmeter barrel exits (Figure 8), the third column is assigned an inner radius equivalent to the connecting rod radius. This nonzero radius is used to signal the difference between open pipe flow and annular flow. Each constant radius section of the connecting rod is represented with a different layer. Changes in the inner radius cause contraction or expansion losses to be calculated; optionally, a net influence of the changing geometry of the connecting rod is simulated to reduce the size of the model. The influence of the wire cable attached to the connecting rod and used to hang the flowmeter in the well is assumed to be negligible and its effect is not incorporated in the model.

In layers that include the barrel, the first column is assigned the radius of the inner barrel diameter and the third column is assigned an inner radius of the barrel outside diameter. The second column is inactive. The second column is only made active for a short layer at the entrance and exit of the flowmeter. These two layers are assigned a large radial conductance value. This layer serves to equilibrate the head values between barrel and bypass flow at the entrance and exit of the flowmeter.

Discussion

The first goal of this study was to determine why the flowmeter measurements acquired at the BHRS indicated an increase in flow rate in a casing joint where there is no inflow and why there was a decrease in inflow just below the casing joints in most cases. The physical basis for these behaviors is depicted in Figure 10.

Consider two points: one located below the flowmeter and one located above it. The pressure loss between these two points is the same whether a path through the flowmeter or around it is followed. With no inflow through the sides of the well at the casing joint, the amount of flow through the flowmeter barrel, which gets measured, is in balance with the flow around the flowmeter, so that the head loss through each path is equal.

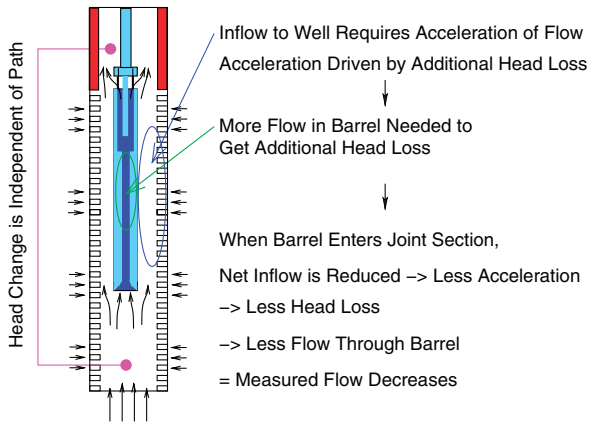

Figure 10. Diagram of physical phenomena influencing flowmeter measurements when inflow to the borehole occurs.

As the top of the flowmeter barrel enters the casing joint, it enters a region where inflow to the well is shut off. To accommodate the smaller acceleration along the sides, there is less flow through the barrel. The measured flow, which is interpreted to be the flow at the entrance of the barrel, drops. As the flowmeter entrance passes through the casing joint, a larger fraction of the barrel is subjected to inflow above the casing joint, resulting in an increase in measured flow. This phenomenon is evident in both the laboratory and the field data.

Some of our laboratory data have inconsistent measurements for different experiments with similar pumping rates. However, all these experiments indicated a drop in measured flow as the top of the flowmeter enters the casing joint. Our field data differ from the laboratory data in that the field data are more repeatable. Reduced noise and repeatability in the field investigation was a significant factor in choosing to use a centralizer rather than a skirt. The field data tend to show a smaller increase rather than a decrease in measured flow when the top of the flowmeter enters the casing joint. For this situation, the difference between a decrease in measured flow in the laboratory data compared with a lessening in the rate of increase of measured flow in the field data may be due to a higher ratio of inflow to borehole flow in the laboratory data.

The second goal of this study was to develop a numerical model of the flowmeter measurements that could be used to infer hydraulic conductivity distributions. We were only partially successful in meeting our second goal. This study has resulted in a numerical model with empirical fitting coefficients. The coefficients apply to aspects of the model that do not have an empirical basis from other well-established sources. As stated earlier, the values used for the coefficients appear to be reasonable. Differences between the laboratory experiments and field data and the inconsistencies of the laboratory data suggest that the empirically based model is not quantitatively accurate for use in analyzing the field data. We expect that more refined laboratory experimentation can provide data to support a more reliable model.

Here we recommend elements of laboratory experimentation to address modeling issues that are not completely resolved by the current experimental data, including fluid mechanics of the flowmeter and screened pipe. Measurement of pressure losses in the annular region between the flowmeter and the screen could advance fundamental knowledge of annular flow where there also is inflow through the screen. Independent control of inflow through the screen would help isolate the flowmeter response from inflow variations. The ideal experiment would also determine the velocity profile of this flow. Such an experimental configuration would allow separation of the influence of the incoming velocity profile from the influence of inflow along the sides of the flowmeter on the division of flow through and around the flowmeter. The influence of inflow variability below the

flowmeter could be investigated through multiple inflow regions with separate flow rate control. Control of inflow to these regions and along the flowmeter barrel would allow the investigation of heterogeneity of inflow on the flowmeter response. Also control of the orientation of the flowmeter with respect to the screen slots would allow testing of the validity of the axial symmetry assumption.

Conclusions

We have provided a physical explanation for why a skirt or packer should be used with a flowmeter. However, this conclusion is problematic with respect to flowmeter use in thick, very permeable aquifers such as the BHRS where (1) relatively high pumping rates are needed to achieve sufficient signal-to-noise ratios and can (2) lead to bypass flow outside the borehole due to borehole flow blockage by the flowmeter. In such cases, bypass flow is aggravated by large aquifer permeability and perhaps, locally, the inherent problem of incomplete collapse around boreholes intended for aquifer characterization (e.g., Dinwiddie et al. 1999; Ruud et al. 1999).

We have created a numerical model of flow in and around the flowmeter that closely reproduces flowmeter responses in solid wall pipes and one of the experiments in screened pipe. Other experiments showed flowmeter responses that were qualitatively similar to the one experiment used to calibrate the flowmeter model but were significantly different quantitatively. We have not established a reason for the differences. The experimental uncertainty implies that the numerical model that is not reliable for field use. Further experimentation could result in a numerical model that is reliable for a flowmeter used with a centralizer rather than a skirt or a packer. A reliable model could increase the flexibility and efficiency of flowmeter use, especially in long-screened wells in relatively high hydraulic conductivity aquifers where signal-to-noise ratios and bypass flow are serious concerns.

Acknowledgments

This work was supported by U.S. Army Research Office Grants DAAH04-96-1-0318 and DAAD19-00-1-0454 and U.S. Environmental Protection Agency Grant X-970085-01-0. Use of the Harry W. Morrison Civil Engineering Building at Boise State University for laboratory space is gratefully acknowledged. The presentation of this work benefited greatly from the careful reviews of Cynthia Dinwiddie and two anonymous reviewers.

References

Arnold, K., and F. Molz. 2000. In-well hydraulics of the electromagnetic borehole flowmeter: Further studies. *Ground Water Monitoring and Remediation*, 20, no. 1: 52–55.

Barrash, W., T. Clemo, J. Fox, and T. Johnson. 2006. Field, laboratory, and modeling investigation of the skin effect at wells with slotted casing, Boise Hydrogeophysical Research Site. *Journal of Hydrology* 326, no. 326: 181–198.

Barrash, W., and E. Reboulet. 2004. *Significance of porosity for stratigraphy and textural composition in subsurface, coarse fluvial deposits; Boise Hydrological Research Site*. *Geological Society of America Bulletin* 116: 1059–1073.

Barrash, W., T. Clemo, and M. Knoll. 1999. Boise Hydrogeophysical Research Site (BHRS): Objectives, design, initial geostatistical results. In *Proceedings of the Symposium on the Application of Geophysics to Engineering and Environmental Problems, Oakland, California*, 389–398, ed. M. Powers, L. Cramer, and R. Bell. Wheat Ridge, Colorado: Environmental and Engineering Geophysical Society.

Barrash, W., and M.D. Knoll. 1988. Design of a research wellfield for calibrating geophysical methods against hydrologic parameters. In Proceedings of the Conference on Hazardous Waste Research, Snowbird, Utah, 296–318. Great Plains/Rocky Mountains Hazardous Substance Research Center, Kansas State University. http://www.engg.ksu.edu/HSRC/98Proceed/.

Century Geophysics Corporation. 2002. 9721 logging tool users guide. http://www.century-geo.com/9721-index.html (accessed 2002).

Clement, W., M. Knoll, L. Liberty, P. Donaldson, P. Michaels, W. Barrash, and J. Pelton. 1998. Geophysical surveys across the Boise Hydrogeophysical Research Site to determine geophysical parameters of a shallow, alluvial aquifer. In *SAGEEP99, The Symposium on the Application of Geophysics to Engineering and Environmental Problems*, ed. M.H. Powers, L. Cramer, L., and R.S. Bell, 399–408. Environmental and Engineering Geophysical Society.

Clemo, T. 2009. Coupled aquifer-borehole simulation. *Ground Water*. In Press.

Clemo, T. 2006. Flow in perforated pipes: A comparison of models and experiments. *SPE Production and Operations*, 21, no. 2: 302–311.

Clemo, T. 2002. MODFLOW-2000 for cylindrical geometry with internal flow observations and improved water table simulation. Technical Report BSU CGISS 02-01, Center for the Investigation of the Shallow Subsurface, Boise State University. http://cgiss.boisestate.edu/pubs/CGISS_Techreports.html.

Cooley, R., and A. Cunningham. 1979. Consideration of total energy loss in theory of flow to wells. *Journal of Hydrology* 43: 161–184.

Crane Co. 1988. Flow of fluids through valves, fittings, and pipe. Technical Paper 410. Long Beach, California: Crane Company.

Dinwiddie, C., N. Foley, and F. Molz. 1999. In-well hydraulics of the electromagnetic borehole flowmeter. *Ground Water* 37, no. 2: 305–315.

Eckhardt, B., T. Schneider, B. Hof, and J. Westerweel. 2007. Turbulence transition in pipe flow. *Annual Review of Fluid Mechanics* 39: 447–468.

Engineering Sciences Data Unit. 1979. Losses caused by friction in straight pipes with systematic roughness elements. Technical Report 79014. London: Engineering Sciences Data Unit.

Harbaugh, A., E. Banta, M. Hill, and M. McDonald. 2000. MODFLOW-2000, the U.S. Geological Survey modular ground-water model—User guide to modularization concepts and the ground-water flow process. Open File Report 00–92. Denver, Colorado: USGS.

Kaleris, V. 1989. Inflow into monitoring wells with long screens. In *Contaminant Transport in Groundwater*, ed. H. Kobus and W. Kinzelbach, 41–50. Rotterdam, The Netherlands: International Association for Hydraulic Research, Balkema.

Michaels, P. 2001. Use of principal component analysis to determine down-hole tool orientation and enhance sh-waves. *Journal of Environmental and Engineering* Geophysics, 6, no. 4: 175–183.

Michaels, P. 1998. In situ determination of soil stiffness and damping. *Journal of Geotechnical and Geoenvironmental Engineering* 124, no. 8: 709–719.
Morin, R., D. LeBlanc, and W. Teasdale. 1988. A statistical evaluation of formation disturbance produced by well-casing installation methods. *Ground Water*, 26, no. 2: 207–217.
Olson, R., and E. Eckert. 1966. Experimental studies of turbulent flow in a porous circular tube with uniform fluid injection through the tube wall. *Journal of Applied Mechanics*, 33, no. 1: 7–17.
Parker, J., J. Boggs, and E. Blick. 1969. *Introduction to Fluid Mechanics and Heat Transfer*. Reading, Massachusetts: Addison-Wesley.
Rouse, H. 1961. *Fluid Mechanics for Hydraulic Engineers*. New York: Dover.
Ruud, N., Z. Kabala, and F. Molz. 1999. Evaluation of flowmeter-head loss effects in the flowmeter test. *Journal of Hydrology* 224: 55–63.
Siwoń, Z. 1987. Solutions for lateral inflow in perforated conduits. *Journal of Hydraulic Engineering* 113, no. 9: 1117–1132.

Appendix

From Momentum Balance to Head Losses

Equation 4 listed the change in momentum of fluid flowing through the volume of fluid inside the screen section as:

$$\frac{D}{Dt}\int_{\mathrm{Vol}} \rho v \,\mathrm{d(Vol)} = \rho 2\pi \int_o^{r_w} v_z^2 r \,\mathrm{d}r\Big|_{z_2} - \rho 2\pi \int_o^{r_w} v_z^2 r \,\mathrm{d}r\Big|_{z_1} + \rho 2\pi r_w \int_{z_1}^{z_2} v_z \cdot v_r \mathrm{d}z \tag{4}$$

Equation 5 presented the forces causing this change in momentum the volume of fluid inside the screen section as:

$$\sum F = -\rho g \pi r_w^2 \Delta z + \pi r_w^2 (P_1 - P_2) - \pi 2 r_w \int_{z_1}^{z_2} \tau_w \mathrm{d}z \tag{5}$$

The following development of Equation 6 is a condensed version of the development presented in Clemo (2009).

The net momentum flux through a cross section of pipe is often written in terms of the momentum factor β, which can be calculated from the laminar velocity profile and is empirical for turbulent flows. The each of the first two terms on the right-hand side in Equation 4 can be replaced using:

$$\beta \rho \pi r_w^2 v_b^2 = \rho 2\pi \int_o^{r_w} v_z^2 r \,\mathrm{d}r \tag{A1}$$

Replacing the first two terms in Equation 4 with Equation A1 and equating Equations 4 and 5 to form a momentum balance equation results in:

$$\begin{aligned} \beta_2 \rho \pi r_w^2 v_{2b}^2 - \beta_1 \rho \pi r_w^2 v_{1b}^2 + \rho \pi 2 r_w \int_{z_1}^{z_2} v_z \cdot v_r \mathrm{d}z \\ = -\rho g \pi r_w^2 \Delta z + \pi r_w^2 (P_1 - P_2) \\ - 2\pi r_w \int_{z_1}^{z_2} \tau_w \mathrm{d}z \end{aligned} \tag{A2}$$

By dividing both sides by ρg, we can convert Equation A2 to be a function of hydraulic head ($h = (P/\rho g) + z$) rather than pressure:

$$\begin{aligned} \beta_2 \frac{\pi r_w^2}{g} v_{2b}^2 - \beta_1 \frac{\pi r_w^2}{g} v_{1b}^2 + \frac{\pi 2 r_w}{g} \int_{z_1}^{z_2} v_z \cdot v_r \mathrm{d}z \\ = \pi r_w^2 (h_1 - h_2) - \frac{\pi 2 r_w}{g} \int_{z_1}^{z_2} \tau_w \mathrm{d}z \end{aligned} \tag{A3}$$

that can be written as:

$$\begin{aligned} h_1 - h_2 = \frac{2}{\rho g r_w} \int_{z_1}^{z_2} \tau_w \mathrm{d}z + \beta_2 \frac{v_{2b}^2}{g} - \beta_1 \frac{v_{1b}^2}{g} \\ + \frac{2}{g r_w} \int_{z_1}^{z_2} v_z \cdot v_r \mathrm{d}z \end{aligned} \tag{A4}$$

τ_w is the average shear stress along the surface of the inner screen. The average shear stress may be written in terms of the Fanning friction factor, f (Cooley and Cunningham 1979; Kaleris 1989).

$$\tau_w = \frac{\rho f v_b^2}{8} \tag{A5}$$

The friction factor is commonly described for a circular pipe by (Parker et al. 1969; Kaleris 1989):

$$\begin{aligned} &f = \tfrac{64}{Re} \; Re < Re_{\mathrm{lam}} \text{ Laminar flow} \\ &f^{-\frac{1}{2}} = -2 \log\left[\tfrac{\varepsilon_p}{3.71} + \tfrac{2.51}{Re} f^{-\frac{1}{2}}\right] Re > Re_{\mathrm{turb}} \text{Turbulent flow} \end{aligned} \tag{A6}$$

where ε_p is the relative roughness of the pipe. The Reynolds number, Re, is defined as $Re = V_b d_h / v$, where v is the kinematic viscosity and d_h is the diameter of the pipe. The transition region between laminar to turbulent flow occurs between $Re_{\mathrm{lam}} > 2000$ and $Re_{\mathrm{turb}} < 4000$. The relation for laminar flow follows from a parabolic velocity distribution and has been verified experimentally. The relation for turbulent flow is known as the Colebrook-White formula (e.g., Rouse 1961). Replacing τ in Equation A4 results in Equation 6.

$$-\Delta h = \int_{z_1}^{z_2} f \frac{v_b^2}{4 r_w g} \mathrm{d}z + \beta_2 \frac{v_{2b}^2}{g} - \beta_1 \frac{v_{1b}^2}{g} + \frac{2}{r_w g} \int_{z_1}^{z_2} v_z \cdot v_r \mathrm{d}z \tag{6}$$